use of prestressed, precast concrete panels in highway bridge construction

Eugene Buth, H. L. Furr, and H. L. Jones
Texas Transportation Institute, Texas A&M University,
H. D. Butler
Texas Highway Department, and
A. A. Toprac
University of Texas at Austin

A beam and slab bridge that makes use of precast, prestressed panels was investigated. For this type of bridge, both the panels and the beams are precast and prestressed in the casting yard. In the bridge structure, the panels span the transverse distance between beams and serve as forms for the cast-in-place portion of the deck. They remain in place to become an integral part of the continuous structural slab. Composite action is obtained when the deck elements and the beams are bonded together by the cast-in-place concrete. Tests were made to determine the ability of this type of bridge to distribute wheel loads in a satisfactory manner and to behave as a composite unit. A full-scale, simple span, prestressed panel concrete bridge was constructed and structurally tested in the laboratory. The bridge was subjected to cyclic applications of design loads and finally to static failure loads. It performed satisfactorily under all load conditions. Several bridges of this type have been in service in Texas for 10 years and have performed well.

•The relatively new type of concrete bridge slab discussed in this paper is constructed of prestressed, precast panels and conventionally reinforced, cast-in-place concrete. This type of construction, shown in Figure 1, reduces construction time and cost.

The precast panels serve as forms for the cast-in-place portion of the deck and remain in place as an integral part of the deck. This eliminates installation and removal of forms and falsework on the underside. The cast-in-place deck is mechanically connected to the beams by the stirrups that extend into the deck as in conventional construction. The cast-in-place concrete is placed over the surface of the panels and into the space above the beams; thereby, all elements are bonded together to act as a composite unit. The cast-in-place concrete serves as the riding surface of the deck.

Two major deviations from conventional beam and slab concrete bridge construction exist in a prestressed panel bridge: bonding of a new concrete to old concrete with sufficient strength to develop an adequate structural connection at the interface and inclusion of transverse joints made by butting adjacent prestressed panels together. The latter created some question on the capacity of the slab to accomplish longitudinal distribution of wheel loads and to resist internal stresses. This transverse joint extends from top to bottom of the prestressed panels but does not extend into the cast-in-place concrete. Present AASHO bridge specifications do not deal directly or by implication with these two structural details.

Figure 1. Prestressed, precast concrete panel bridge.

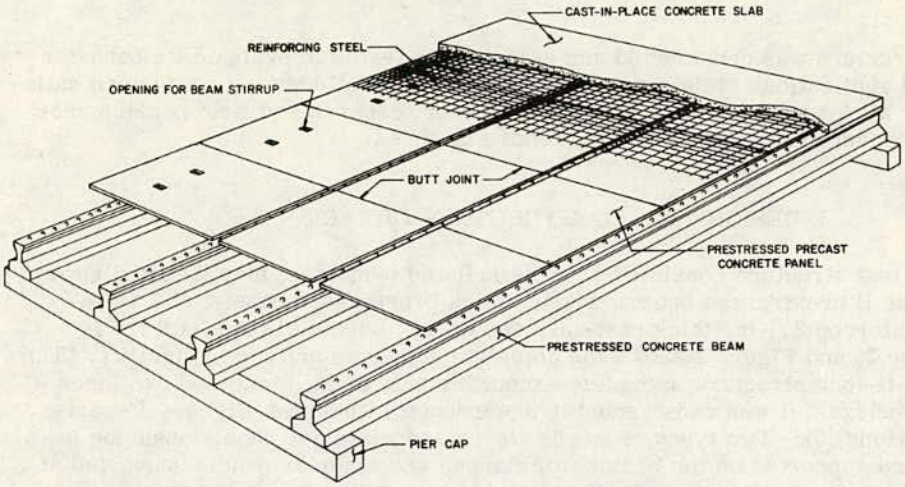

Figure 2. Layout of prestressed panel bridge.

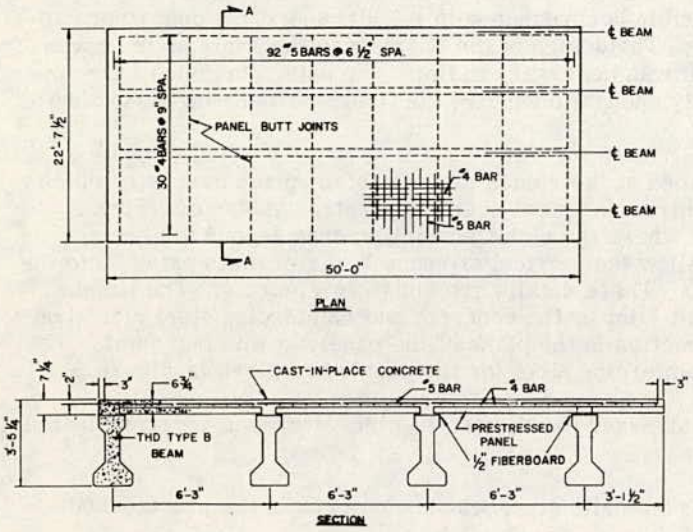

Figure 3. Full-scale bridge structure and testing facility.

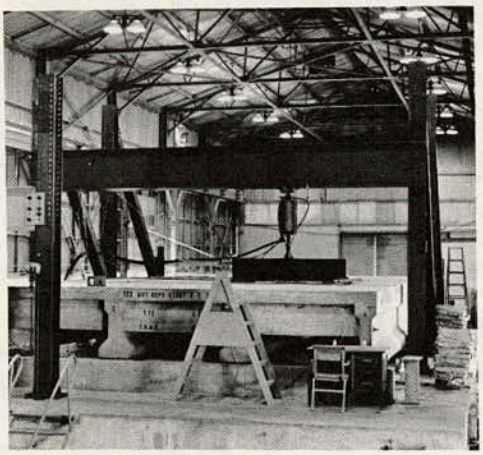

A full-scale structure was constructed and structurally tested to evaluate its behavior under repeated applications of design loads and static failure loads. It performed satisfactorily under all load conditions. Further details of research and field performance of prestressed panel bridges are given elsewhere (2, 3, 4).

DESIGN AND CONSTRUCTION DETAILS

The full-scale test structure consisted of two simulated bent caps, four Texas Highway Department type B prestressed beams, 3¼-in.-thick prestressed panels, and a conventionally reinforced 3½-in.-thick cast-in-place deck. Layout of the structure is shown in Figure 2, and Figure 3 shows the complete structure and testing facility. The 23-ft-wide, 50-ft-long structure, complete except for side rails, simulated two lanes of a four-lane bridge. It was constructed in accordance with Texas Highway Department specifications (5). Two types of panels were used: interior panels spanning between beams and supported on the beams' top flanges and exterior panels supported at one end on a beam and continuous over the outside beam with a 2½-ft overhang. The panels became an integral part of the continuous deck when the top portion of the deck was cast.

The entire structure was designed in accordance with AASHO specifications, where applicable, for an HS20-44 loading. The design of the beams was the same as in conventional construction, except that it was necessary to finish the outer portions of the upper surface of the top flange smoothly enough to receive the fiberboard seating strip shown in Figure 2.

The prestressed panels were joined at their ends by the cast-in-place concrete, which engaged a 3-in. extension of prestressing steel over the prestressed beams (Fig. 4). At the outside edge of the bridge where the slab was cantilevered beyond the beam, holes were cast in the panel to allow the vertical stirrups in the beam to extend into the cast-in-place portion of the slab. These details are shown in Figure 4. The panels were joined at the transverse butt joint by the concrete and reinforcing steel placed on top of them. There was no connection in the plane of the panels at this butt joint. Dimensions and details of the reinforcing steel for the panels are given in Figure 5.

The design of the composite prestressed panel, cast-in-place deck was governed by the following requirements:

1. Under construction loads, no tensile stresses should occur in the prestressed panel,
2. The minimum transverse bending moment capacity of the composite section should be greater than or equal to the AASHO design moment (3.77 kip-ft/ft), and
3. No transverse tensile stresses should occur in the panel under service loads.

These requirements were satisfied by a 3¼-in.-thick panel with prestressing as shown in Figure 5 and a 3½-in.-thick cast-in-place slab with the transverse reinforcing shown in Figure 2. Although the design thickness of the composite slab was 6¾ in., the actual slab measured 7 in. Properties of the concrete are given in Table 1.

It was assumed in the design that all elements of the structure would act as a composite unit. This assumption required that all elements of the structure be bonded together in a suitable manner to transfer all stresses across the interface between the cast-in-place deck and the prestressed panels and at the slab-beam interfaces. At the interfaces, the same proven methods used in conventional beam and slab bridges were employed. Three methods, used as test variables, were employed to bond the cast-in-place concrete to the top surface of the prestressed panels (Fig. 6). Z-bars (Fig. 7) were used to provide both shear and tensile bond over a selected portion of the deck. In another area, portland cement grout was thoroughly brushed onto the rough surfaces

Figure 4. Detail of slabs resting on (a) interior beam and (b) exterior beam.

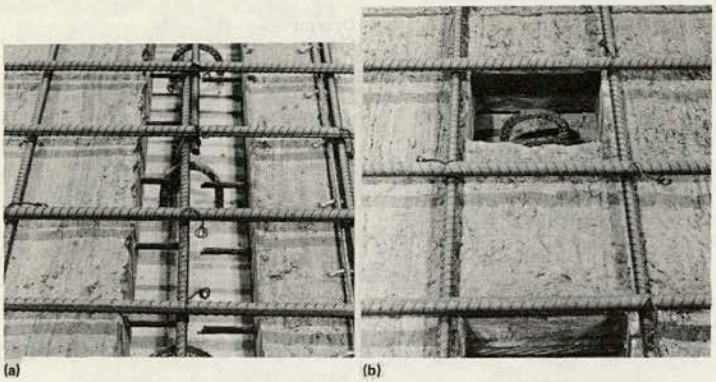

Figure 5. Details of (a) interior panels and (b) exterior panels of full-scale bridge.

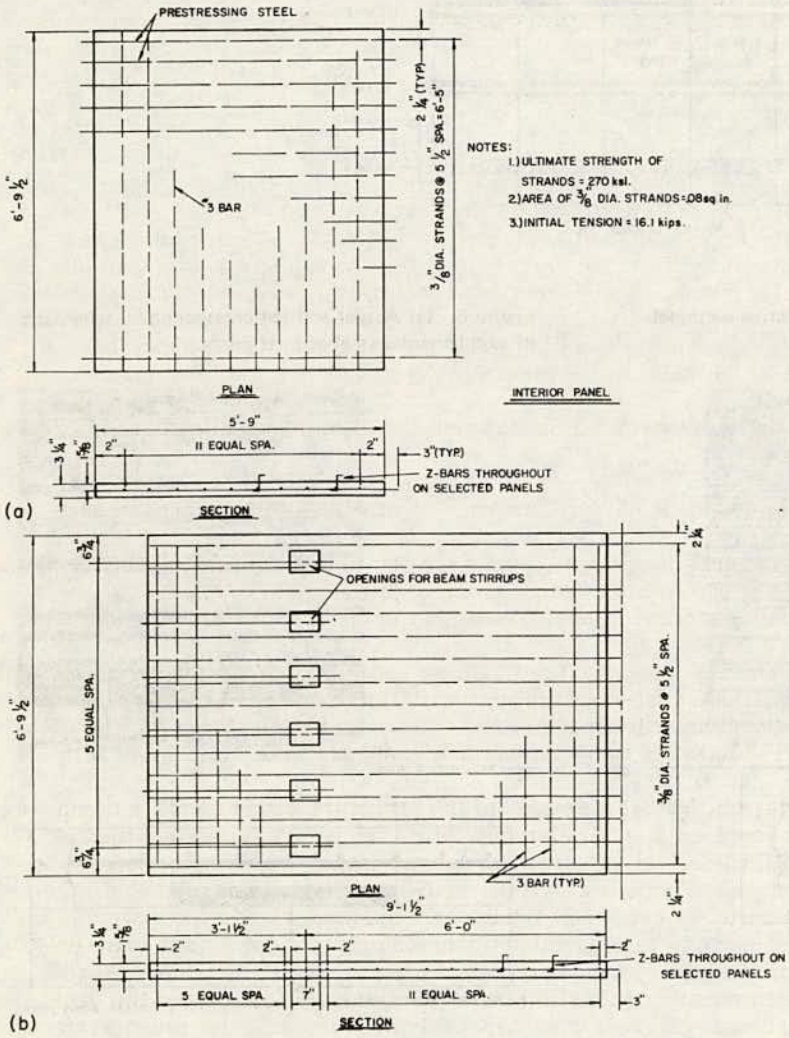

Table 1. Concrete properties.

Item	Date Cast	Release Strength (psi)	Compressive Strength (psi)	Tensile Strength (psi)	Dynamic Modulus of Elasticity (psi × 10^6)
Prestressed beams	10-29-70	4,810	7,590 at 28 days		6.19
	10-30-70	4,880	7,130 at 28 days		6.19
Prestressed panels	12-10-70	—[a]	8,550 at 316 days	640 at 480 days	5.65
Cast-in-place deck	2-25-71		5,970 at 240 days	490 at 400 days	5.23

[a]Data not available.

Figure 6. Location and identification of variable sections.

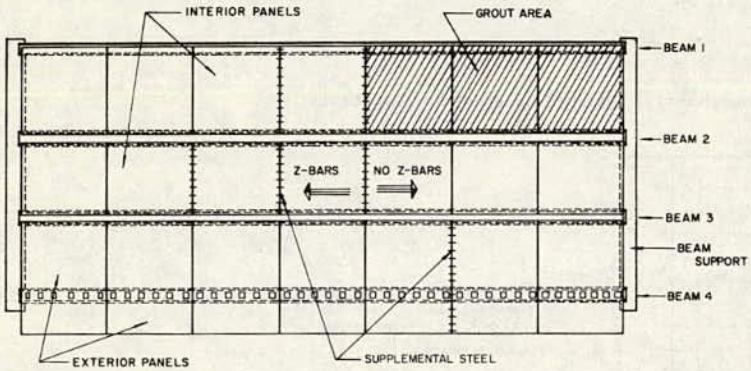

Figure 7. (a) Actual and (b) cross-sectional schematic of Z-bars.

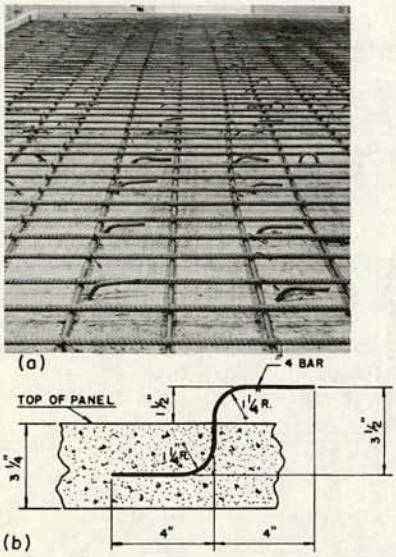

Figure 8. (a) Actual and (b) cross-sectional schematic of supplemental steel at butt joints.

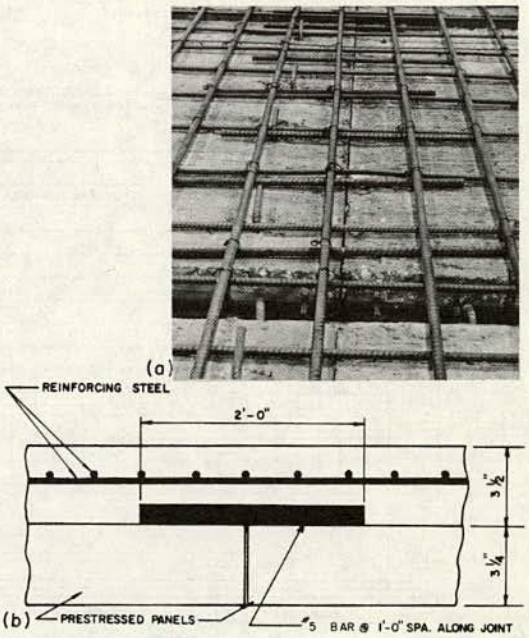

of the panels to serve as a bonding agent. The cast-in-place deck was placed over the grout. There was no special treatment over the remainder of the deck. The locations of these areas on the structure are shown in Figure 8. The surface of the panels was thoroughly cleaned with water from a hose and nozzle and then damp-dried shortly before placement of the cast-in-place concrete. The grout was applied on the selected panels immediately before concrete placement. The progress of the grout brushing operation was regulated so that the grout did not dry before placement of the concrete.

At selected transverse butt joints, supplemental bars were placed on the surface of the panels and extended across the butt joint (Fig. 8). They were intended to aid in transferring a wheel load across the panel joint and in distributing it in the longitudinal direction of the bridge.

INSTRUMENTATION

Instrumentation was planned to detect any breakdown in the overall performance of the full-scale bridge and to reveal any local failure that might develop in the vicinity of the applied loads. The structure was instrumented with mechanical gauges for measuring deflection and for detecting relative movement between elements and with electrical resistance gauges for measuring strains in the beams and deck. Strain gauges were mounted on the top of the slab, bottom of the prestressed panel, and on the top and bottom of the beams. The slab gauges were in areas of maximum shear and bending to provide information that would indicate bond failure between slab and panel if such developed at the gauge (Fig. 9).

Linear motion dial gauges were installed to detect any relative vertical motion between abutting prestressed panels and to detect relative transverse and longitudinal movement between the prestressed panels and beams. Relative vertical movement between adjacent panels would indicate either a vertical crack through the cast-in-place slab above the panel joint or bond failure between the panel and cast-in-place slab. Either of these vertical movements would indicate a local deficiency in the structure. Any relative horizontal movement between the beam and the slab would indicate a failure of the bond betweeen these two elements.

LOADING SYSTEM

Two types of loading arrangements were used to simulate design loads. Simulation of axle loads was accomplished with the hydraulic ram and loading pad arrangement. The two pads representing the dual wheels of a single axle of a design HS20 truck were 12 in. by 20 in. in plan and spaced 6 ft on centers. A loading beam spanned between these two pads and the loading ram was positioned at midspan of the beam. A hydraulic testing machine operated a ram for both the static and dynamic axle loadings. The system produced a nearly sinusoidal loading for these particular tests.

Simulation of a wheel load rolling across a transverse butt joint between prestressed panels was accomplished with two hydraulic rams acting on loading pads positioned on opposite sides of and adjacent to the transverse joint. The load alternated between the two rams, and one ram loaded and unloaded while the other remained inactive. The pulsator used to produce this alternating wheel loading produced a nearly trapezoidal load-time trace.

The static failure load tests were conducted by using the same load pad but with a 400-kip hydraulic ram substituted for the dynamic loading ram.

The procedure for evaluation of the behavior of the structure under cyclic loading was as follows:

Figure 9. Layout of electrical resistance and beam deflection gauges.

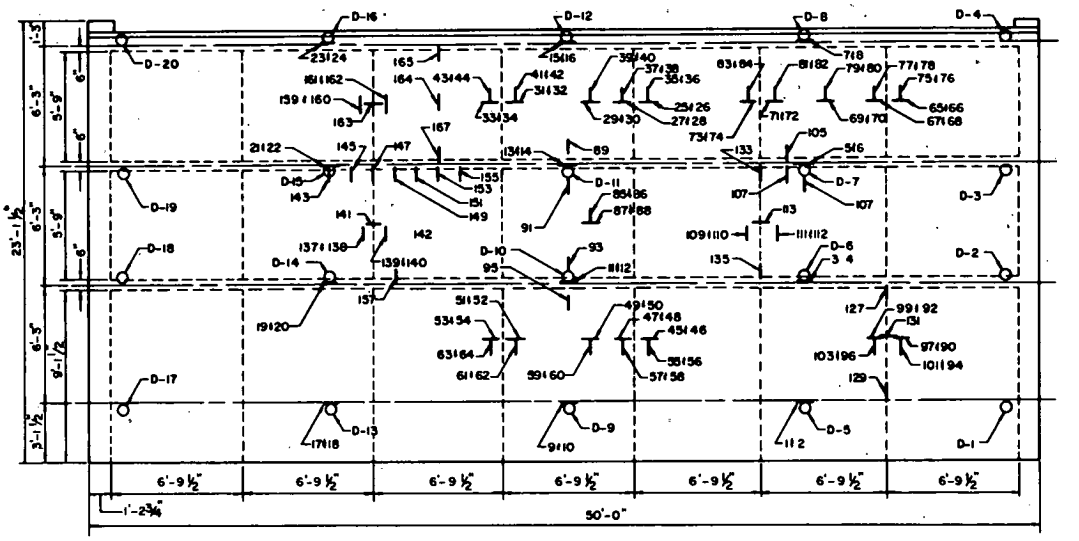

Table 2. Loads applied to structure.

No.	Type	Purpose
1	Cyclic axle	To determine behavior of bond between panel and cast-in-place concrete with Z-bars and dowels, but no grout
2	Cyclic axle	To determine behavior of bond between panel and cast-in-place concrete with Z-bars, but no dowels or grout
3	Cyclic axle	To determine behavior of bond between panel and cast-in-place concrete with no Z-bars or dowels; one wheel pad was on grouted area, and the other was not
4	Cyclic, alternating wheel	To determine ability of deck to support load simulating wheel crossing joint between two panels with no dowels or Z-bars
5	Static wheel	To determine failure load of the structure in an area with no dowels or Z-bars
6	Static wheel	To determine failure load of the structure in an area with no dowels or Z-bars
7	Static wheel	To determine failure load of the structure in an area with Z-bars, but no dowels
8	Static wheel	To determine failure load of the structure in an area with Z-bars and dowels

Figure 10. Position of load applications.

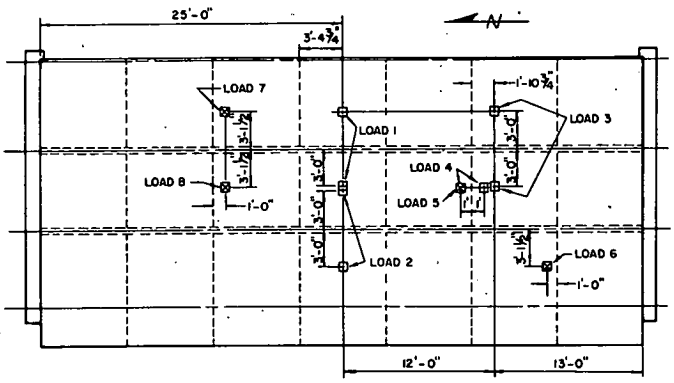

1. Determine the response to a static design load by reading the strains and deflections at all gauge locations.
2. Subject the structure to a number of cycles of load.
3. Again determine the response to static load.
4. Visually inspect the structure each time the static load is applied to determine whether any form of distress has occurred.
5. Compare the responses to static loads obtained in 1 and 3 above to determine whether any distress has occurred in the structure.

PROGRAM OF TESTS

The structure was subjected to cyclic design loads and, after completion of these, to static failure loads. In the application of the cyclic loads, the condition of the structure was determined by periodically measuring its response to static load. Gauge readings under application of a static load were made before the cyclic loading, at predetermined intervals during loading, and after loading at each load position.

The loading plan, designed to accomplish a complete evaluation of the structures, is given in Table 2. The positions of the loads on the full-scale bridge model are shown in Figure 10. Loads 1 through 3 were cyclic loads and simulated an AASHO design axle load plus impact of 41.6 kips. Load 4 was a cyclic load and alternated on either side of a panel butt joint to simulate an AASHO design wheel load plus impact of 20.8 kips rolling across the joint. Loads 6, 7, and 8 were static failure loads.

RESULTS AND DISCUSSION

Repetitive Load Tests

The condition of the structure during cyclic loading was monitored by periodically determining structural response to a static load. A change in the response to a static load was considered to be the result of a change in the structural integrity of the bridge. Comparisons of beam deflections under static load before loading and after 2 million cycles indicated that no distress was caused by the loading. This is further supported by the fact that no slippage occurred between the beams and the slab as determined by the relative displacement dial gauges between those elements.

Experimentally measured strains at the upper and lower surface of the slab at locations in the proximity of the simulated wheel pads are given in Tables 3, 4, and 5. The generally close agreement between values obtained from the static load response tests (48 kips) made before and after cyclic loading indicate that no distress was caused by the loading.

Strain readings made before and after application of load 4, a 20.8-kip cyclic alternating wheel load, are given in Table 6. It is observed that the average ratio of strain readings after cyclic loading to readings before cyclic loading is 1.00 for data obtained with load on the north ram and 0.97 with load on the south ram. Closer observations of the individual gauge readings do not indicate any consistent trends in the data for load on the north ram, but do indicate a possible trend in the data for load on the south ram. The after-before ratios are consistently low for the top gauges and high for the bottom gauges. However, the largest difference in strains is only 22 μin./in., and this is not considered to be conclusive evidence of distress. No distress was observed visually, and none was indicated by data from static failure load test 5.

Prior to application of load 3, minute cracks were discovered above some transverse joints between panels. The widths of these cracks were measured with a microscope and were found to be 0.002 in. and less. These cracks were not found upon inspection

Table 3. Experimental strains for load position 1.

Gauge		Strain (μin./in.)	
Placement	No.	Before	After
Longitudinal	25	-11	-15
	26	-26	-17
	27	-14	-13
	28	-20	-14
	29	-56	-56
	30	+1	-2
	31	-16	-14
	32	-19	-15
	33	-15	-14
	34	-16	-13
Transverse	35	-18	-23
	36	+14	+26
	37	-39	-27
	38	+20	+33
	39	-74	-76
	40	+61	+74
	41	-28	-24
	42	+25	+36
	43	-39	-38
	44	+18	+24

Table 4. Experimental strains for load position 2.

Gauge		Strain (μin./in.)	
Placement	No.	Before	After
Longitudinal	45	-9	-5
	46	-15	-14
	47	-3	-4
	48	-17	-14
	49	-32	-32
	50	+7	+1
	51	-7	-7
	52	-23	-19
	53	-23	-24
	54	-23	-19
Transverse	55	-21	-21
	56	+22	+24
	57	-31	-27
	58	+47	+34
	59	-77	-62
	60	+75	+76
	61	-32	-29
	62	+31	+36
	63	-11	-12
	64	+25	—[a]

[a]No data.

Table 5. Experimental strains for load position 3.

Gauge		Strain (μin./in.)	
Placement	No.	Before	After
Longitudinal	65	-4	-10
	66	-8	-14
	67	-6	-11
	68	-10	-18
	69	-12	-18
	70	-13	-21
	71	-13	-18
	72	-3	-20
	73	-16	-25
	74	+3	+3
Transverse	75	-7	-14
	76	+13	+9
	77	-12	-20
	78	+17	+13
	79	-52	-59
	80	+53	+51
	81	-50	-58
	82	+66	+56
	83	-54	-57
	84	+50	+40

Figure 11. Comparison of theoretical and experimental bending stresses in (a) transverse and (b) longitudinal directions.

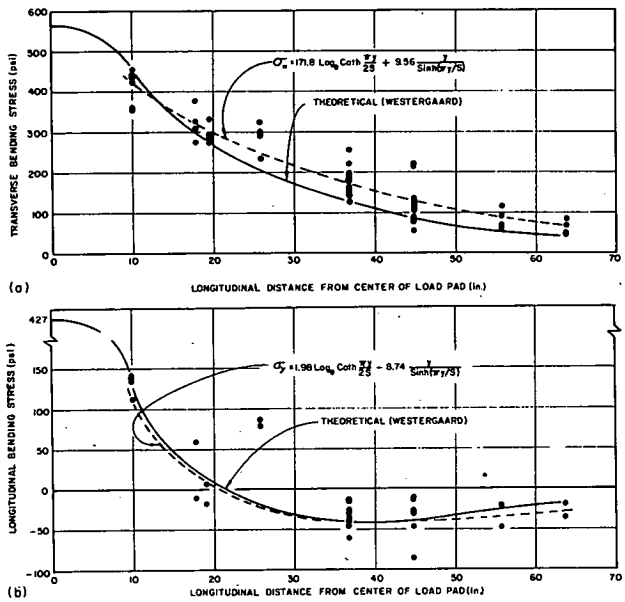

Table 6. Experimental strains (in μin./in.) for load position 4.

	North Ram			South Ram		
Gauge	Before Loading	After 2,000,000 Cycles	After / Before	Before Loading	After 2,000,000 Cycles	After / Before
109	-94	-97	1.03	-71	-60	0.84
110	+74	+74	1.00	+56	+63	1.13
111	-76	-70	0.92	-100	-78	0.78
112	+62	+63	1.02	+81	+92	1.14
113	-88	-92	1.05	-99	-95	0.96
Avg			1.00			0.97

after conclusion of load 2. Some cracks were in the vicinity of a panel joint near the north end of the bridge, far removed from the loads, and it is believed that they were caused by shrinkage, thermal strains, or both, and not by load. A limited number of core samples taken after completion of the testing program indicated that some of the cracks extended as deep as 2 in. below the surface, lacking at least 1½ in. of penetrating through the cast-in-place slab.

Comparisons of stresses computed from measured strains obtained during the static load response tests with those predicted by theory (6) are shown in Figure 11. Stresses were computed from the measured slab strains by using the plane stress relationships:

$$\sigma_L = \frac{E}{1 - \mu^2} (\epsilon_L + \mu \epsilon_T) \quad (1)$$

$$\sigma_L = \frac{E}{1 - \mu^2} (\epsilon_T + \mu \epsilon_L) \quad (2)$$

where

σ_L = stress in the longitudinal direction of bridge,
σ_T = stress in the transverse direction of bridge,
ϵ_L = strain in the longitudinal direction,
ϵ_T = strain in the transverse direction,
E = 52.3 and 56.5 psi for cast-in-place and prestressed panel concrete, and
μ = 0.15.

As expected, these stresses were observed to consist of a combination of benging stresses and in-plane or membrane stresses in the slab resulting from overall bending of the entire structure. These components of stress were separated mathematically in the following manner. The values of the component of bending stresses attributable to bending of the composite structure, at the top and bottom surface of the slab, were assumed to be proportional to the distances of these two surfaces from the neutral surface of the composite unit. The components of stress resulting from local bending of the slab were arbitrarily assigned equal values, of opposite sign, at the top and bottom surface of the slab. This allowed a unique solution for the distribution of the total stresses into the two components. Stresses computed from strain measurements made both before and after cyclic loading in each case were used for these computations.

Relationships presented by Westergaard (6) with adjustments for 50 percent edge fixity of the slab were used in arriving at the theoretical curves. These stresses on both the top and bottom surfaces were assigned the same sign as the bending moment at that point—compression on the top surface being positive moment. Curves were fitted to the experimental data by the method of least squares to facilitate comparisons between experimental and theoretical values. The function chosen to fit the experimental values was based on the form of the theoretical expressions for bending moments:

$$\sigma = C_1 \log_e \coth \frac{\pi y}{2s} + C_2 \frac{y}{\sinh \frac{\pi y}{s}} \quad (3)$$

where C_1 and C_2 were constants determined from the least squares fit. Equation 3 is shown in dashed lines in Figure 11. The maximum difference between the theoretical curve and the least squares fit to the data for transverse bending is about 45 psi and is less than 15 psi for longitudinal bending. It is further noted that at points close to the load, where maximum stresses occur, comparisons are very good.

Static Failure Load Tests

The static failure loads were applied in 10-kip increments, and strain and deflection

Figure 12. Crack pattern that developed during static failure load tests.

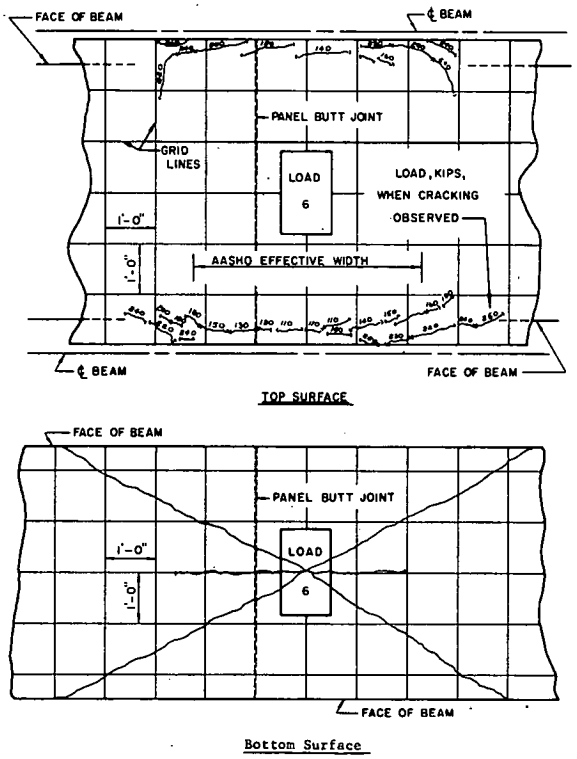

Table 7. Summary of static failure load test results.

Load Position	Date Tested	Cracking Load (kips)	Failure Load (kips)	Failure Mechanism	Remarks
5	3-9-72	90	270	Punching shear	Significant flexural distress had occurred
6	2-17-72	110	280	Punching shear	Significant flexural distress had occurred
7	4-6-72	120	250	Punching shear	Truncated pyramid did not fully develop in adjacent panel
8	3-23-72	80	260	Punching shear	Significant flexural distress had occurred

Figure 13. Comparison of experimental and theoretical failure load values.

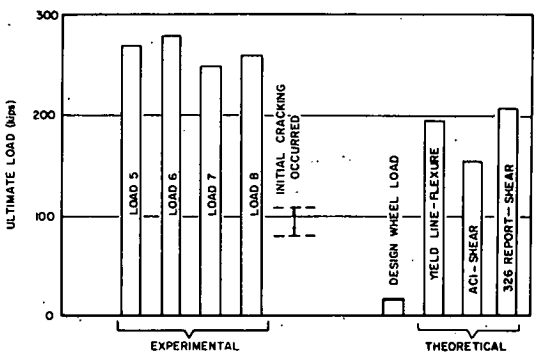

gauge readings were made after each load increment. Cracking in the concrete in each test was first detected on the upper surface of the slab. These cracks occurred in the negative moment regions, on either side of the load, above the inside faces of the adjacent beams. The cracking load varied from 80 to 120 kips for the four tests. Cracking was observed on the lower surface of the slab, under the load pad, at a load 20 to 30 kips higher than the load causing the first top surface crack. With additional loading, the cracks on both surfaces grew until the load reached 220 to 240 kips. At this load, the rate of progression of the cracks slowed considerably, almost ceasing to extend but opening wider with additional load. The upper surface cracks generally extended parallel to the beams and eventually began turning away from the beam into the span of the slab being loaded. The lower surface cracks crossed to form an X under the load and extended until they reached the beams. A third crack, much shorter in length, passed through the center of the X and extended parallel to the beams. Additional load increments were applied until a punching shear failure occurred in each case. A typical pattern of the flexural cracking is shown in Figure 12.

The ultimate failure surface formed a truncated pyramid, typical of a punching failure in a slab. In tests 5, 6, and 8, the surface showed no apparent influence of the panel butt joint. However, in test 7, one segment of the surface intersected a panel joint and did not develop in the adjacent panel.

A summary of the static failure load test results is given in Table 7. A comparison of experimental and theoretical values of failure load is shown in Figure 13. A yield line analysis, using a two-fan failure mechanism, was made to determine the theoretical load (7). This mechanism and its dimensions were selected on the basis of the cracking pattern that was observed in the tests. In this analysis, the slab was transformed into an equivalent orthotropically reinforced slab (7). The ultimate load was computed to be 195 kips. Because the failure mode obtained experimentally was not a flexural failure, it can only be said that the ultimate flexural failure load for this slab was greater than the values attained when the punching shear failure occurred. It was expected that the predicted flexural failure load from the yield-line analysis would be greater than the 280 kips obtained experimentally, particularly since the analysis results in an upper bound solution. However, this is seen not to be the situation.

The first and most obvious factor that could have caused the actual flexural strength of the slab to be greater than that predicted by the yield-line analysis is the enhancement of the strength of the slab by in-plane compressive stresses. Such stresses existed in the longitudinal direction of the slab because the entire structure bent as a composite unit. Another source of in-plane compressive stresses has been observed in lightly reinforced slabs where the failure mechanism is confined to an interior portion of the slab (7). With application of a concentrated load and partial development of the failure mechanism, in-plane extension of the slab occurs in the area of the failure mechanism. This extension is restrained by the surrounding portion of the slab, and compressive in-plane stresses are thereby created in the area of the failure mechanism. This phenomenon, in a rigidly restrained slab, was observed by Wood (7) to increase the flexural strength of a lightly reinforced slab by 10.9 times. This same phenomenon also enhances the punching shear capacity of a slab.

The AASHO code relationship between a wheel load and the maximum slab bending moment for this structure is $M = 0.18P$. If this relationship is used along with the ultimate moment capacity of the section, an ultimate wheel load can be calculated. This load is somewhat meaningless because the load-moment relationship is intended for an elastic slab, and the relationship would be disrupted by yielding and redistribution of stresses. Nonetheless, such a calculation results in an ultimate load of 123 kips.

The shear strength of concrete slabs is a very complex subject and at present is handled with semiempirical methods of analysis. The primary difficulties are the lack of understanding of the behavior of concrete under multiaxial states of stress and the inability

to determine the state of stress at any given point in a concrete slab. An analysis of the slab studied here is further complicated by the use of both prestressed and conventionally reinforced concrete. The American Concrete Institute code provisions for slabs and footings specify that the nominal shear stress for two-way action (neglecting the capacity reduction factor) be computed by $v_u = V_u/bd$, and this shear stress is specified not to exceed $4\sqrt{f_c'}$. If the average value of compressive strength for the slab from Table 1 is used, this method predicts the ultimate load, V_u, as 140 kips if a panel butt joint is assumed and 156 kips if no joint is assumed. The experimental failure surface did not intersect the panel joint in tests 5, 6, and 8, and the results of these tests should be compared with the predicted value of 156 kips. It should be realized that the ACI code provision is a simplified design equation intended to provide a lower bound on the ultimate load. An equation (8) that more closely approximates the lower bound of experimental data is

$$v_u = 4(d/r + 1)\, f_c' \tag{4}$$

where

d = effective depth of the slab and
r = side dimension of the loaded area.

This equation results in an ultimate shear strength of 457 psi if the average compressive strength for the slab is used. The resulting ultimate punching shear loads are 186 and 210 kips for an assumed joint and no assumed joint respectively. Experimental values, given in Table 7, exceed these theoretical values by 25 to 35 percent. Experimental values given in the ACI committee report (8) exceed the theoretical values by 0 to 100 percent.

Three bridges of this type, located in Grayson County, Texas, were built in the early 1960s and have been serving satisfactorily since then. A visual inspection of these bridges was conducted in the first phase of this study (2), and crack patterns on the deck surfaces were mapped. Cracking above the panel joints was found on only two of the bridges. These cracks were rather extensive in some areas and extended to about half the depth of the cast-in-place concrete. Although they are undesirable from a durability standpoint, especially in severe climates, they have not damaged the structural integrity of these bridges. Load tests were performed, and core samples were taken from one of the bridges to determine the condition of the bond between prestressed panels and cast-in-place deck. This examination indicated no further distress in the bridges nor any signs of bond failure.

SUMMARY AND CONCLUSIONS

A single-span, full-scale, prestressed panel bridge was evaluated experimentally in the laboratory. The structure was subjected to cyclic applications of design load plus impact and to static failure loads. It performed satisfactorily under all test conditions.

Theory presented by Westergaard (6) (the basis of present design specifications) predicts local bending stresses in the slab of the structure studied with reasonable accuracy if in-plane stresses resulting from spanwise bending of the entire structure are ignored.

Two million applications of simulated design axle load plus impact were accomplished at three locations on the bridge structure. The bond at the interface between the prestressed panels and the cast-in-place concrete performed without any indication of distress under these cyclic loads.

Two million cycles of design wheel load plus impact alternating on opposite sides of a panel butt joint were applied at one location on the structure without causing distress. Satisfactory performance was exhibited by the bridge slab when subjected to static failure loads. The lowest value of cracking load measured experimentally was 3.8 times the design wheel load plus impact, and the lowest measured ultimate load was 12 times the design wheel load plus impact.

The failure surfaces that developed in the static failure tests intersected and continued across the panel to the cast-in-place interface and were not influenced by the interface.

The following conclusions were drawn from the results of the experimental work reported.

1. The bond at the interface between the prestressed, precast panels and the cast-in-place concrete performed without any indication of distress under cyclic design loads and static failure loads.
2. No distinction in performance among those areas of the deck with mechanical shear connectors (Z-bars), with grouting treatment, and without special treatment could be made after 2 million applications of design load or static failure load tests.
3. Wheel loads were transferred and distributed across transverse panel butt joints in a satisfactory manner. Those joints with supplemental reinforcing gave no indication of superior performance under 2 million applications of design wheel load or static failure loads when compared to those joints without supplemental steel.
4. With this type of construction, some small transverse cracking in the cast-in-place deck over panel butt joints is to be expected as a result of thermal and shrinkage effects. Such cracks have not been found to be detrimental to the overall performance of a bridge.

REFERENCES

1. Standard Specifications for Highway Bridges, Tenth Ed. American Association of State Highway Officials, 1969.
2. Jones, H. L., and Furr, H. L. Study of In-Service Bridges Constructed With Prestressed Panel Sub-Deck. Texas Transportation Institute, Texas A&M Univ., Res. Rept. 145-1, July 1970.
3. Jones, H. L., and Furr, H. L. Development Length of Strands in Prestressed Panel Sub-Decks. Texas Transportation Institute, Texas A&M Univ., Res. Rept. 145-2, Dec. 1970.
4. Buth, E., Furr, H. L., Jones, H. L., and Toprac, A. A. Evaluation of a Prestressed Panel, Cast-In-Place Concrete Bridge. Texas Transportation Institute, Texas A&M Univ., Res. Rept. 145-3, Sept. 1972.
5. Standard Specifications for Road and Bridge Construction. Texas Highway Department, Austin, Jan. 1962.
6. Westergaard, H. M. Computation of Stresses in Bridge Slabs Due to Wheel Loads. Public Roads, Vol. 11, No. 1, March 1930.
7. Wood, R. H. Plastic and Elastic Design of Slabs and Plates. Ronald Press Co., New York, 1961.
8. Shear and Diagonal Tension. Proc., ACI Jour., Vol. 59, Nos. 1-3, Jan.-March 1962, pp. 1-30, 277-334, 352-396.